Research Article

# Biogenic preparation of biphasic calcium phosphate powder from natural source of snail shells: bioactivity study

Edwin A. Ofudje[1] · Fatai Akinwunmi[2] · Ezekiel F. Sodiya[1] · Samson O. Alayande[3] · Abimbola A. Ogundiran[4] · Gabriel O. Ajayi[5]

Received: 24 March 2021 / Accepted: 15 March 2022
Published online: 11 April 2022


**Abstract**
In this present work, carbonated apatite powder (CAP) and β-tricalcium phosphate (β-TCP) were prepared from waste snail shells via thermal decomposition followed by chemical precipitation method with phosphoric acid in a one step process. The CAP produced was thereafter reacted with a pore forming agent solution of ammonium bicarbonate to formed carbonated apatite powder- ammonium bicarbonate scaffold composites (CAP-AMB) and was deployed in a bioactivity experiment with simulated body fluid (SBF) media. The phase purity, crystallinity, particle size, thermal behaviour, elemental composition, morphology as well as the functional groups of snail shells, synthesized CAP and CAP-AMB scaffold were assessed by XRD, FE-SEM, TGA, EDX, TEM and FT-IR. XRD and selected area electron diffraction (SAED) results confirmed the synthesized apatite as pure amorphous powder which upon heat treatment, transformed to polycrystalline powder. Analysis of FT-IR results revealed that the apatite produced from snail shells (SS) contains phosphates and hydroxyl functional groups. Furthermore, the formation of carbonated apatite was also confirmed from the FT-IR result with peaks which appeared at 882 and 1484 $cm^{-1}$ respectively, thus depicting a B-type apatite. Microscopy analyses by FE-SEM and TEM indicated that the prepared apatite is composed of different morphologies in the range of 5 to 200 nm long. The presence of trace elements such as K, C, Na, Mg and Mg which could play crucial functions in biological applications were detected by EDX measurement alongside Ca and P. The mixture of CAP with AMB produced interconnected pores structure with porosity in the range of 35–67%. The bioactivity study of the SBF treated CAP-AMB composite confirmed apatite formation on the scaffold surface which totally covered the pores after seven days of incubation. Thus, waste biomaterial of snail shells origin can be use for the production of pure apatite that could be useful in medical application.

✉ Edwin A. Ofudje, ofudjeandrew4real@yahoo.com; eaofudje@mtu.edu.ng | [1]Department of Chemical Sciences, Mountain Top University, Prayer City, Ogun State, Nigeria. [2]Department of Chemistry, Federal University of Agriculture, Abeokuta, Ogun State, Nigeria. [3]Department of Physical Science, First Technical University (Tech-U), Ibadan, Nigeria. [4]Department of Chemical Sciences, Tai Solarin University of Education, Ijebu-Ode, Ogun State, Nigeria. [5]Department of Biological Sciences, Mountain Top University, Prayer City, Ogun State, Nigeria.

**Graphical abstract**

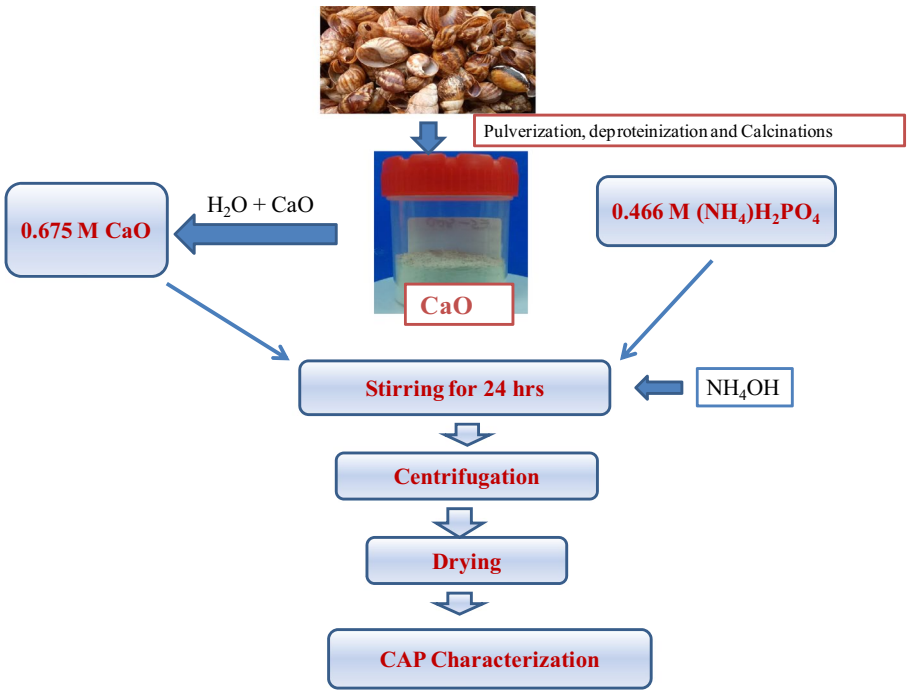


**Keywords** Apatite · Bioactivity · Calcinations · Carbonated powder · Snail shells

## 1 Introduction

Carbonated apatite powder (CAP) ceramics are widely recognized as potential substitute to auto- and allograft materials for bone replacement as a result of their chemical resemblance with the constituent of hard tissues and bones in mammals [1–3]. Individual age is a major factor in determining the amount of carbonate found in human bone and could be around 2–8 wt.% [2, 3]. In the apatite structure, carbonate group can either replace the phosphate group leading to the formation of A-type or the hydroxyl functional group to form B-type carbonate apatite [2–4]. Report has it that both A- and B-types of substitution can take place simultaneously resulting in the formation of mixed AB-type substitution [2, 4]. The presence of cation ($Ca^{+}$ and $Ca^{2+}$) and anions ($PO_4^{3-}$ and $OH^{-}$) in the structure of the apatite permits such substitutions in the apatite and as a result of this, different kinds of elements or ions can be introduced into the lattice of the apatite including carbonate ions [5, 6]. The incorporation of little amount of cations or anions into the lattice of the apatite usually cause considerable changes in the physicochemical properties such as morphology, crystallinity, surface charge as well as the stoichiometry which allows variations in the physicochemical activities of the apatite [5]. According to Le Geros [7], decrease in the crystallinity of apatite coupled with an increase in solubility was noticed when both in vivo and in vitro assays were carried out in the apatite structure as a result of the occurrence of a B-type carbonate.

The control of the amount of carbonates release or loss during sintering at higher temperature is very difficult as a result of the volatile nature of carbon(IV) oxide gas for those apatite synthesized chemically [6]. Biological apatites produced from natural sources contain carbonates as derived from their respective raw materials which make them more thermally stable when compared with those synthesized chemically during heat treatment. For instances, Venkatesan et al. [8] reported the fabrication of carbonated hydroxyapatite powder from Thunnus obesus bone using thermal calcinations at 900 °C for 5 h and 2 M NaOH alkaline hydrolysis. XRD investigation of raw bone showed the formation of poorly crystalline hydroxyapatite which is entrenched in organic medium. In the study carried out by Suresh et al. [9], snail shell was successfully utilized for the synthesis of hydroxyapatite nanorods powder which was identified to be hexagonal crystal of B-type carbonated HA. Adeogun et al. [10] transformed

waste egg shell into a nano-rod carbonated hydroxyapatite by wet chemical precipitation process with Ca/P ratio of 1.95. Mustaffa et al. [11] fabricated spherical carbonated hydroxyapatite of Ca/P ratio less than 1.68 and with sizes in the range of 4.03–10.4 µm from the calcinations of cockle shells which was followed by sol–gel precipitation. Sea shells were utilized by Santhosh and Prabu [12] via calcinations and wet chemical precipitation for the development of clean crystalline HAp produced at 250 °C but at a more elevated heat treatments, β-TCP HAp was produced. Red algae *C. officinalis* was utilized in the synthesis of different phases of hydroxyapatites including carbonated apatite [13]. Ofudje et al. [6] reported the potential of pig bone waste as source of material for the extraction of carbonated apatite through thermal decomposition at a temperature range of 600–1000 °C. Rosita and Yusril [14] reported the use of *Cerastoderma edule*, *Paphia undulata*, and *Meretrix meretrix shells* for the preparation of carbonated hydroxyapatite (CHAp) by precipitation method of Ca/P ratio to be around 1.75–1.77 with carbonate content of 3.10–4.05wt.%. The effective application of snail shells for the production of nanorods β-type carbonated hydroxyapatite was reported by Kumar et al. [15]. Chinese mystery snail shells were recycled as calcium source in the preparation hydroxyapatite as documented by Huan et al. [16]. The shells were initially decompose at 860 °C to form porous CaO and thereafter, hydrothermally utilized to synthesize HA using different phosphate sources.

Snail (*Archachatina marginata*) is widely consumed and served as a significant and essential part of daily diet across the length and breadth of Nigeria due to its nutritive values and softness which is mostly recommended for the elderly and people with chronic diseases. Snail is reported to contain almost all the amino acids needed for human nutrition and therefore has a wide local and international utilization in West Africa, Asia and Western Europe where it is popular [17]. In Nigeria, the demand for snail outweighs the supply due to the fact that it is not available throughout the year. A popular news paper in 2018 reported that the annual requirement for snail in Nigeria worth about 7.5 million kg and that the United States of America imports more than $4 million worth of snails annually from all over the world, including Nigeria [18]. Snail shell with little or no economic value constitutes the discarded waste parts of snails are often generated by snail sellers, eateries, or restaurants which could pose serious degree of environmental challenges [19]. After the consumption of the edible parts of the snails, the shells are thrown away indiscriminately thus constituting environmental nuisance but these waste shells can be effective utilized as starting materials for the production of other valuable products and thus bring immense economic prosperity to snail shells [19, 20]. For instance, snail shells have been reported for waste water treatments [21], applied in the productions of biomaterials and drugs in medicine [22] and utilized extensively as effective reinforcement material in the production of composites [19, 23].

This present research work aimed at considering snail shells waste as source of carbonated apatite extraction, thus improving the values of perceived agro-waste. The structure of the agro-waste derived carbonated apatite powder was elucidated with XRD, FT-IR, FE-SEM, EDX, TEM and TGA/DTA analyses. The CAP produced was thereafter mixed with ammonium bicarbonate (AMB) for the formation of carbonated scaffolds. The CAP-AMB was deployed in biological study using simulated body fluid (SBF) media for seven day incubation at a temperature of 37 °C.

**Table 1** Chemical reagents and purities used in preparing SBF media [34]

| Order | Chemical formula | Amount | Purity (%) |
|---|---|---|---|
| 1 | NaCl | 8.035 g | 99.5 |
| 2 | $NaHCO_3$ | 0.355 g | 99.5 |
| 3 | KCl | 0.225 g | 99.5 |
| 4 | $K_2HPO_4.3H_2O$ | 0.231 g | 99.0 |
| 5 | $MgCl_2{\cdot}6H_2O$ | 0.311 g | 98.0 |
| 6 | 1.0 M HCl | 39 ml | – |
| 7 | $CaCl_2$ | 0.292 g | 98.0 |
| 8 | $Na_2SO_4$ | 0.072 g | 99.0 |
| 9 | Tris | 6.118 g | 99.0 |
| 10 | 1.0 M HCl | 0-5 ml | – |

## 2 Experimental procedure

### 2.1 Chemicals

$NH_4OH$ (99.99%) and $NH_4H_2PO_4$ (98%) were obtained from Merck, while the likes of (NaCl, $NaHCO_3$, KCl, $K_2HPO_4.3H_2O$, $MgCl_2{\cdot}6H_2O$, HCl, $CaCl_2$, $Na_2SO_4$, tris) and NaOH were purchase from Sigma-Aldrich and their purity are as listed in Table 1.

### 2.2 Collection and preparation of calcium oxide

Snail shells (SS) were collected and the impurity present were mechanically cleaned from the surface. The remaining impurity present (protein) were removed by boiling in hot water and 0.1 M NaOH solution for 40 min, followed by

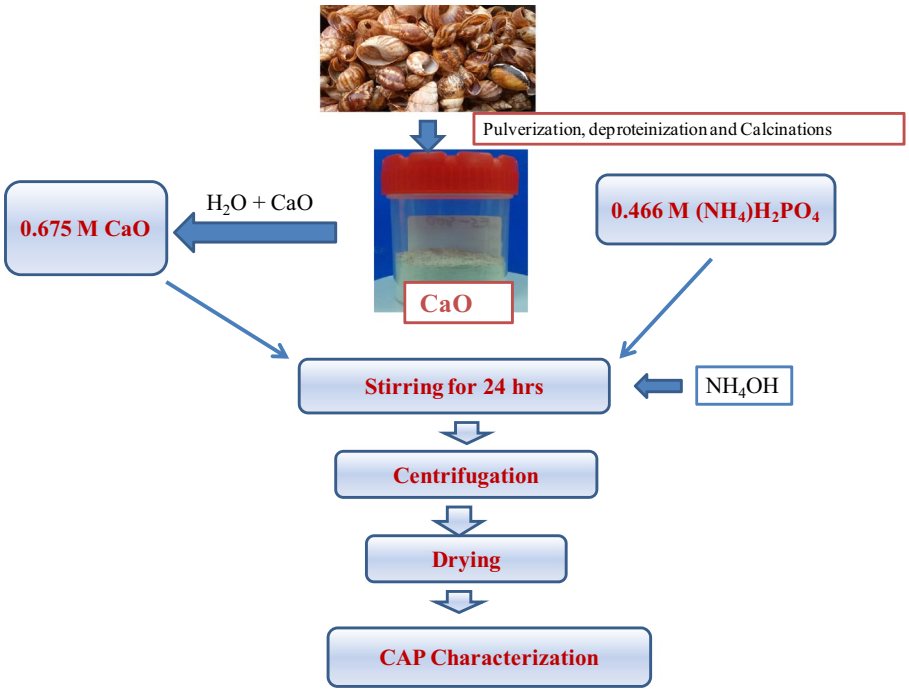


**Fig. 1** Flow chart for the synthesis of CAP from snail shell

oven drying at 100 °C for 12 h and thereafter calcined in an air atmosphere at 800 °C to get rid of any organic matters and for the formation of calcium-oxide following the method described by Santhosh and Prabu [12].

### 2.3 Synthesis of carbonated apatite powder

Calculated amount of the CaO powders produced from the snail shells was exothermically reacted with ammonium diphosphate solution drop wisely. The mixtures were allowed to age for 24 h on a magnetic hot plated with constant stirring at a speed of 150 rpm and at room temperature to avoid agglomeration. The solution was sustained at a pH of 11 with the introduction of $NH_4OH$ solution. The content was thereafter filtered using centrifuge and washed severally with ultra pure water and oven dried at 80 °C over night. The flaky apatite formed was turned into powder form via pulverization. The prepared powder was then sintered at a temperature of 1000 °C and then characterized using different analytical techniques. The schematic diagram for the fabrication of carbonated apatite powder from snail shells is depicted in Fig. 1. The snail shell was converted to CaO using equation while the CaO so produced was converted to CAp using Eq. 2 [24] as follows:

$$CaCO_3 \rightarrow CaO + CO_2 \quad (1)$$

$$10CaO + 6(NH_4)_2HPO_4 \rightarrow Ca_{10}(PO_4)_6(OH)_2 + 8H_2O + 12NH_3 \quad (2)$$

### 2.4 Scaffold preparation and bioactivity assay

Scaffolds apatite was obtained by adopting the method previously discussed by Ofudje et al. [6, 25]. Briefly, various weight of the as-prepared carbonated apatite was mixed with ammonium bicarbonate (AMB) (serving as the pore forming agent) in the ratio of 100:0; 10:90, 20:80, 30:70, 40:60 and 50:50 in terms of percentage CAP to AMB. Thereafter, the mixtures were compressed to form pellets using hydraulic press and calcined at a temperature of 1000 °C. Products obtained were elucidated with scanning electron microscope, while the pores formed were evaluated with mercury porosimeter. The bulk density, densification and porosity of the scaffolds were determined using the methods previously described [6].

Calculation of densification of the scaffold was achieved via Eq. 3 [6]:

$$Densification = \frac{B.D}{T.D} \times 100 \quad (3)$$

Given that *B.D* is the sintered density and *T.D* denotes the theoretical density.

*B.D* was determined from Eq. 4 [6]:

$$B.D = \frac{m}{V} \quad (4)$$

where *m* is the mass of the scaffold in *g* and *V* stands for the volume in $cm^3$ of the CAP-AMB scaffold. The porosity of CAP-AMB scaffold prepared was evaluated using Eq. 5 below [6]:

$$Porosity = \left(1 - \frac{B.D}{T.D}\right) \times 100 \quad (5)$$

The bioactivity investigation of the fabricated scaffold carbonated apatite was performed in simulated body fluid (SBF). Details about the composition and preparations of SBF solution were documented by Kokubo and Takadama, [26], which was adopted in this work. An abrade bottle containing 150 ml SBF solution and scaffolds pellets of carbonated apatite was placed in a water bath shaker at 37 °C for one week, thereafter, the samples were removed, rinsed with distilled water and dried. SEM and FT-IR analytical tools were both used to examine the variations at the surface of the immersed pellets.

### 2.5 Structural elucidation

The crystallography study as revealed by X-ray diffraction analysis of snail shells, CaO and the fabricated CAP were collected between the angle range of $2\theta = 10–60°$ using monochromatic radiation of Cu Kα (1.5406 A°) with the aid of PANalytical (X'Pert PRO, Netherland). Crystallographic identification was done using the pattern of JCPDS data in comparison with the experimental XRD values. Bruker Optics, TENSOR 27 series FT-IR spectrometer was recorded using the KBr pellet technique in the region of 4000–400 $cm^{-1}$ with 4 $cm^{-1}$ resolution. The surface morphology was done with the aid of field emission scanning electron microscope (FE-SEM) using a Carl Zeiss Supra 55VP microscope using an accelerating voltage of 0.1–30 kV. The morphological feature was examined further using transmission electron microscope (TEM; Tecnai 20 G2 FEI, Netherland). Energy Dispersive X-Spectroscopy (EDX) (Hitachi, Japan, S-3000H electron microscope with accelerating voltage of 15 kV) was used to studied the elemental composition of the fabricated apatite. Thermal stability of prepared sample was analyzed using SDT Q600 V8.3 Build 101simultaneous DSC-TGA.

## 3 Results

### 3.1 Structural elucidation

Figure 2 depicts the crystallography of uncalcine and calcined snail shells. The XRD pattern of uncalcine snail shell

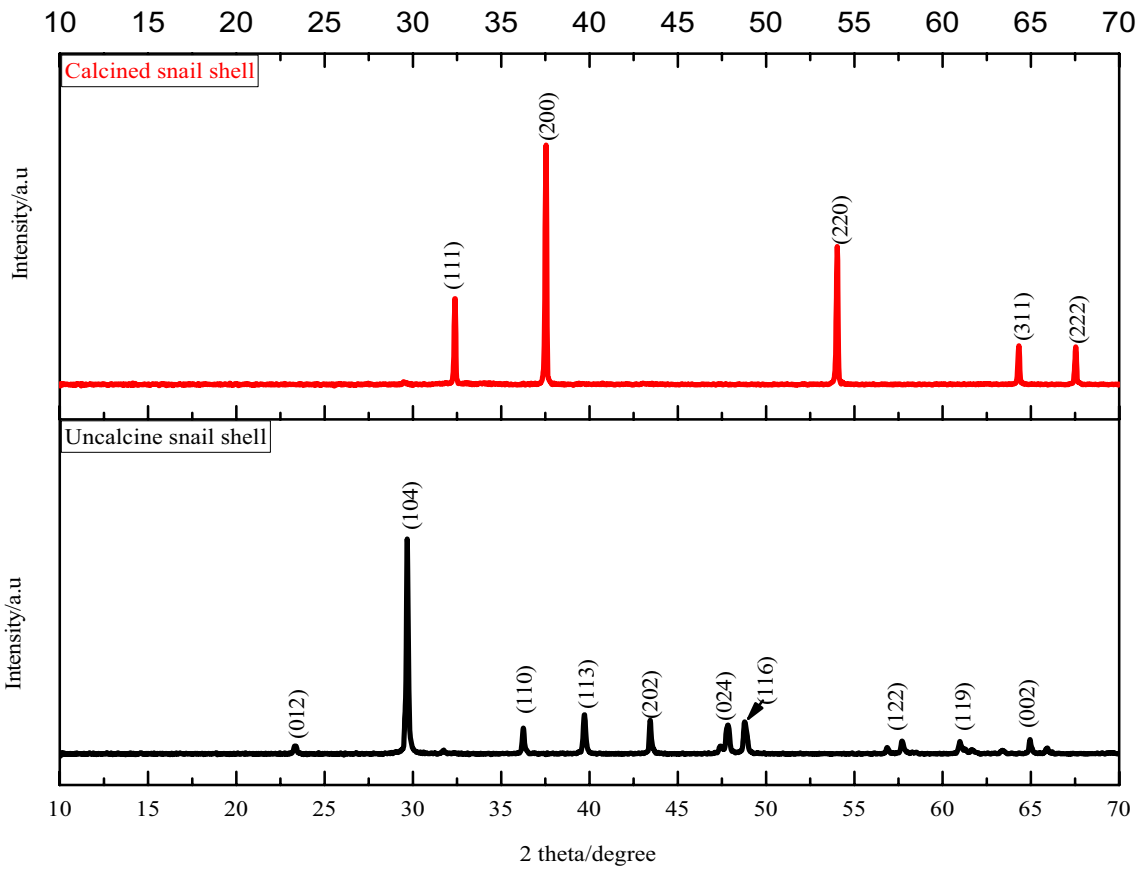


**Fig. 2** XRD analysis of raw snail shells and calcined snail shells

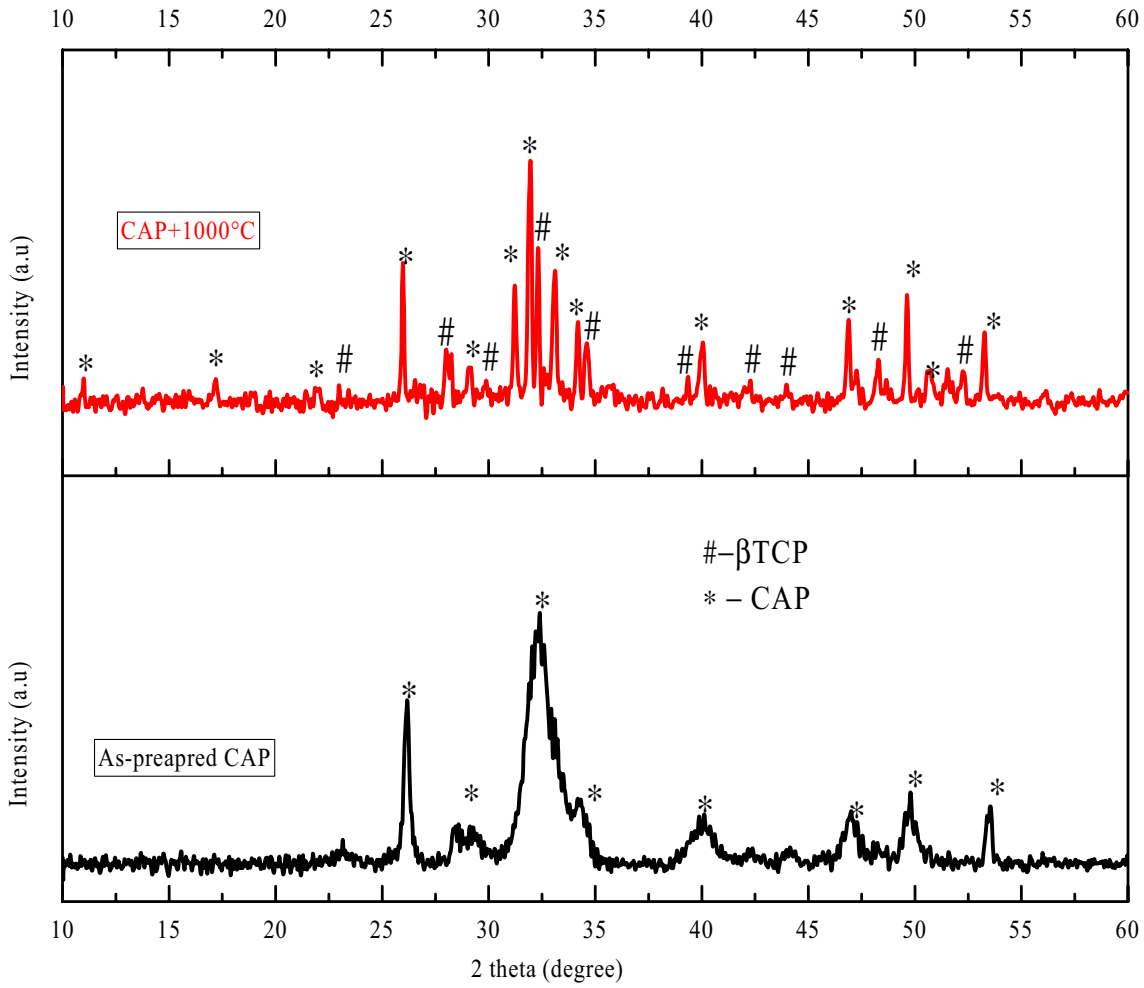


**Fig. 3** XRD analysis of as-prepared carbonated apatite and heat treated carbonated apatite at 1000 °C

powder confirmed to be calcium carbonate (calcite) with JCPDS file no. 47-1743. This suggests that the raw snail shells are mainly composed of crystalline phase of calcite ($CaCO_3$). The phase composition of the calcined snail shells were determined to be calcium oxide by JCPDS file no. 37-1497 with the appearance of peaks at $2\theta = 37.23°$ and 54.06° corresponding to (200) and (220) planes. This clearly confirmed the transformation of the raw snail shells (calcite) into calcium oxide at higher calcinations temperature. The XRD powder patterns obtained for the as-synthesized CAP from calcined snail shells and sintered apatite are as shown in Fig. 3. The various peaks detected were matched with standard values from JCPDS file no. 09-432. Only peaks corresponding to monophasic apatite powder were identified by the JCPDS file data in both as-prepared and sintered CAP, indicating the formation of pure apatite powder. Minor characteristic peaks corresponding to β-tricalcium phosphate (β-TCP) phase was seen along with CAP phase after heat treatment at 1000 °C. The formation of β-TCP could be due to calcinations at high temperatures. According to El Brick-BenAbdeslam et al. [27], trace amount of β-TCP presence with HAp could be due to the removal of small amount of water molecules and/or carbonation of $CaCO_3$ or CaO. Laonapakul et al. [28] observed similar behaviour when they reported the production of β-TCP with a small amount of HAp via manually mixing with the aids of a mortar and pestle between $CaCO_3$ or CaO and DCPD and a solid-state reaction at 1100 °C. In this present study, the decreases in the vibration of $OH^-$ group from the FT-IR analysis of CAP (Fig. 5) upon heat treatment, clearly suggests the lost of water molecules from the apatite structure thus leading to the formation of β-TCP along with the CAP phase. Peaks broadening are indicative of poorly crystalline or an amorphous nature of the as-prepared apatite. However, the emergence of lots of sharp peaks at a higher temperature of 1000 °C signifies the production of polycrystalline apatite and this was also confirmed by TEM result in Fig. 6c, d. Similar observations were reported when waste pig bone [6] and egg shells [10] were used. Scherrer's equation was

used to estimate the average crystallite size of the fabricated apatite [29]:

$$D_{(hkl)} = \frac{K\lambda}{\beta \cos\theta} \tag{6}$$

Given that the crystallite size in nm is represented by $D$, $\beta$ (in degree) stands for full width at half maximum (FWHM) of the peak intensity, diffraction wavelength (0.154 nm) is given by $\lambda$, while $\theta$ stands for diffraction angle, the constant which relates to the crystallite shape is denoted by $K$ and is around 0.94. The crystal parameters which express the relationships between crystal plane indexes were computed from the following equation since hydroxyapatite is a hexagonal crystal [6, 29]:

$$\frac{1}{d_{(hkl)}} = \left\{ \frac{4\left(h^2 + k^2 + kh\right)}{3a^2} + \frac{l^2}{c^2} \right\}^{1/2} \tag{7}$$

Given that $d$ denote the Miller indices (h k l) in nm and the parameters of the lattice are given as a, b and c which measures the dimensions of the unit volume. The hexagonal unit cell volume (V) was estimated with the use of the equation [10]:

$$V = 2.589(a^2).c \tag{8}$$

The plane of Bragg's angle diffraction at (211) was used for this purpose. It was found that the size of the as-prepared CAP was 27 nm and 76 nm for sintered CAP. The grain growth observed after heat treatment at 1000 °C suggests enhanced crystallite size after heat treatment. The computed lattice constants (a and c) and unit cell volume are 0.9425, 0.6880 and 1.5843 nm respectively. The elemental analysis of uncalcined and calcined SS powders are as showed in Fig. 4 which revealed feature bands of carbonate ions ($CO_3^{2-}$) at 714, 874 and 1473 $cm^{-1}$ respectively [30]. The broad band observed at 1473 $cm^{-1}$ signifies the existence of carbonate groups [30]. The peaks found at 3594 $cm^{-1}$correspond to the vibration of $OH^-$ which disappeared after calcinations of the raw snail shells. The elemental investigation of as-prepared and sintered apatite powders are shown in Fig. 5. Distinctive vibrational peaks of the phosphate, $PO_4^{3-}$ and hydroxyl, $OH^-$ groups were prominent. Peaks observed at 488, 571 and 1085 $cm^{-1}$ was assigned to absorption bands of phosphate group in

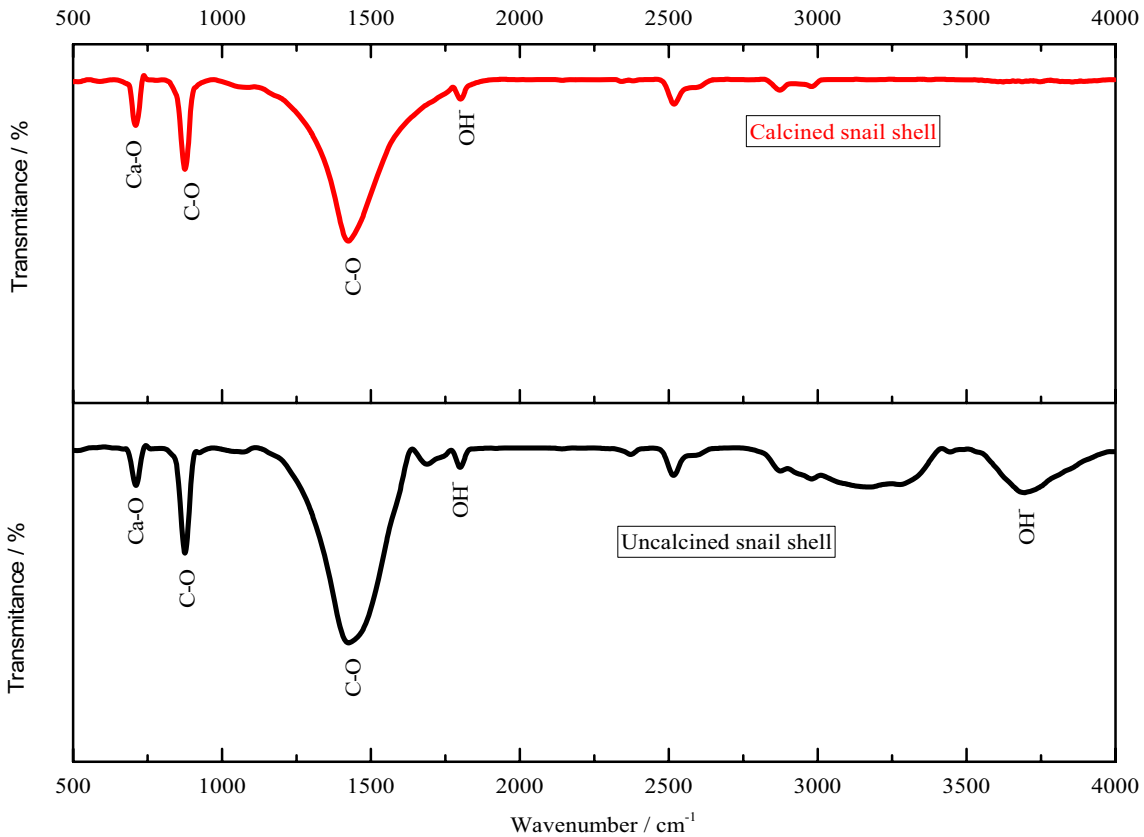


**Fig. 4** FT-IR spectral of raw snail shells and calcined snail shells

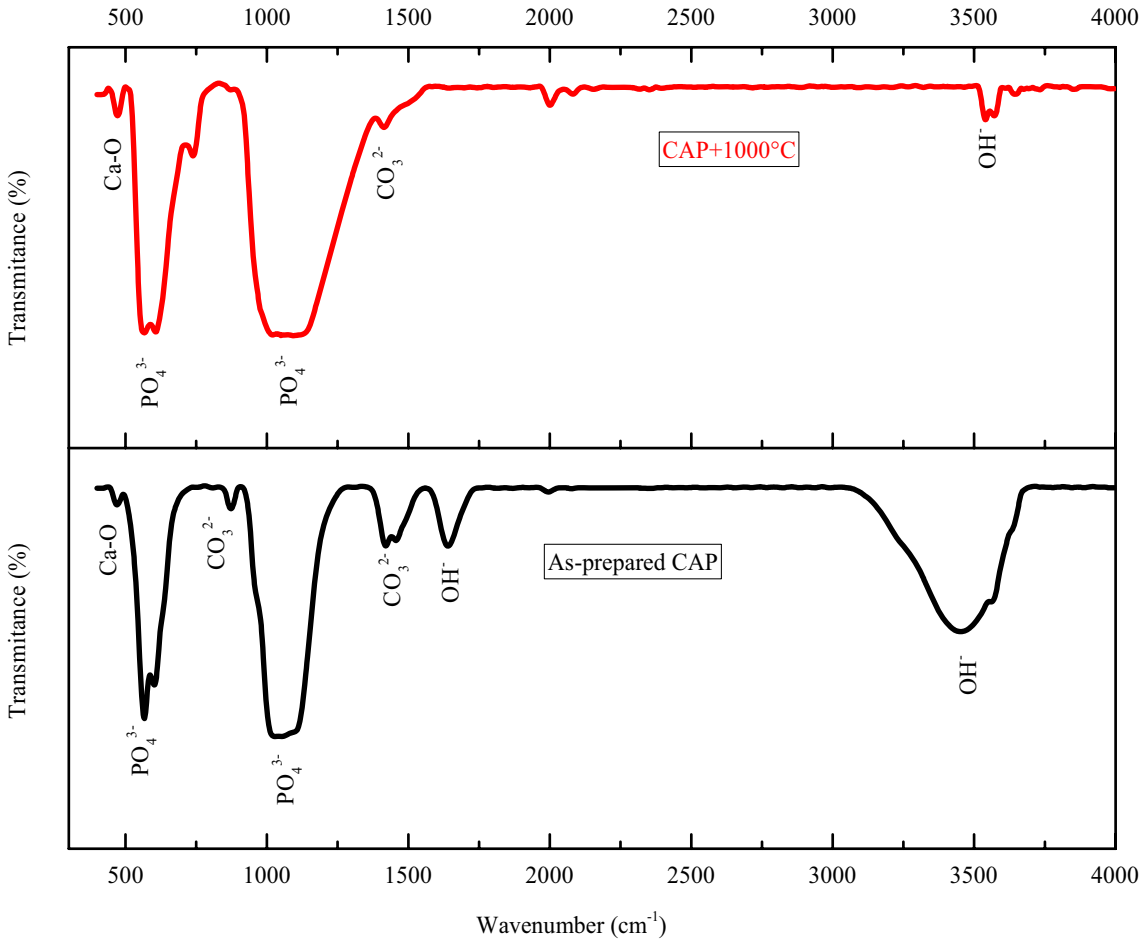


**Fig. 5** FT-IR spectral of as-prepared carbonated apatite and heat treated carbonated apatite at 1000 °C

CAP [9]. The band at 3562 $cm^{-1}$ is owing to the vibration of $OH^-$ group of CAP which decreases upon heat treatment thus confirming the decomposition of the apatite to β-TCP. The presence of peaks at 882 $cm^{-1}$ as well as the one observed at 1484 $cm^{-1}$ was attributed to $CO_3^{2-}$ vibrations.

Figure 6a illustrates the FE-SEM of the calcined snail shell which shows a flake-like morphology. A careful examination of the sintered calcium phosphate by FE-SEM shows different particle sizes and shapes (rod-like, capsule-like and round shapes) crystals with size ranging from 5 to 220 nm long and 10–16 nm wide for the prepared CAP (Fig. 6b). A similar pattern was observed using TEM analysis which corroborate the morphological result of the FE-SEM to be rod-like in shape with size 67–200 nm long and 20–40 nm wide (Fig. 6c). Selected area electron diffraction (SAED) investigation in Fig. 6d showed spotted sharp and unbroken rings indicating a polycrystalline apatite which corroborate XRD results. Figure 7a shows the EDX measurement of calcine snail shells which revealed that the calcite is composed of oxygen (37.57 wt.%), calcium (58.83 wt.%), carbon (3.32 wt.%) and magnesium (0.28 wt.%). The EDX measurement of fabricated CAP is as presented in Fig. 7b which revealed that the apatite consisted of oxygen (49.79 wt.%), calcium (25.02 wt.%), phosphorous (17.53 wt.%), carbon (3.89 wt.%) and magnesium (3.77 wt.%). The existence of these trace metals could enhanced the biological applications of the apatite. For instance, the important role of $Na^+$ and $Mg^{2+}$ ions in the development of bone and teeth was documented by Mohammad et al. [31], while bone loss and fragility could be the adverse effect of their absence. The non-stoichiometric amount of the prepared CAP was achieved and this is related to the calcium deficiency in the molar ratio of the mixed powders of the starting materials. In the literature report by Safronova et al. [32], it was observed that calcium deficient hydroxyapatite produced consisted of two main phases of HAp and β-TCP with Ca/P molar ratio of the starting materials between 1.48 and 1.67. It might be inferred therefore; that the CAP produced is non-stoichiometric based on the Ca/P molar ratio (Ca/P = 1.45) of the mixed powders.

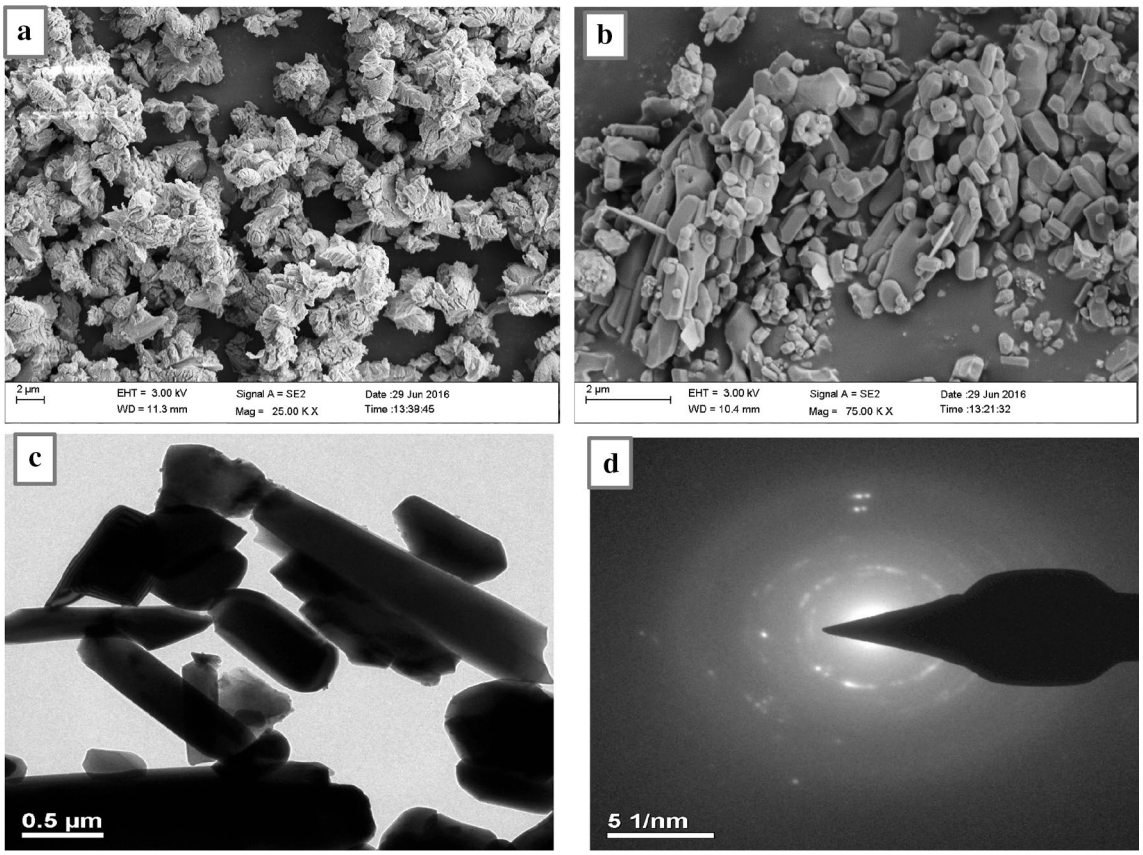


**Fig. 6** FE-SEM images of **a** snail shell powder, **b** carbonated apatite, **c** TEM image and **d** SEAD of carbonated apatite powder

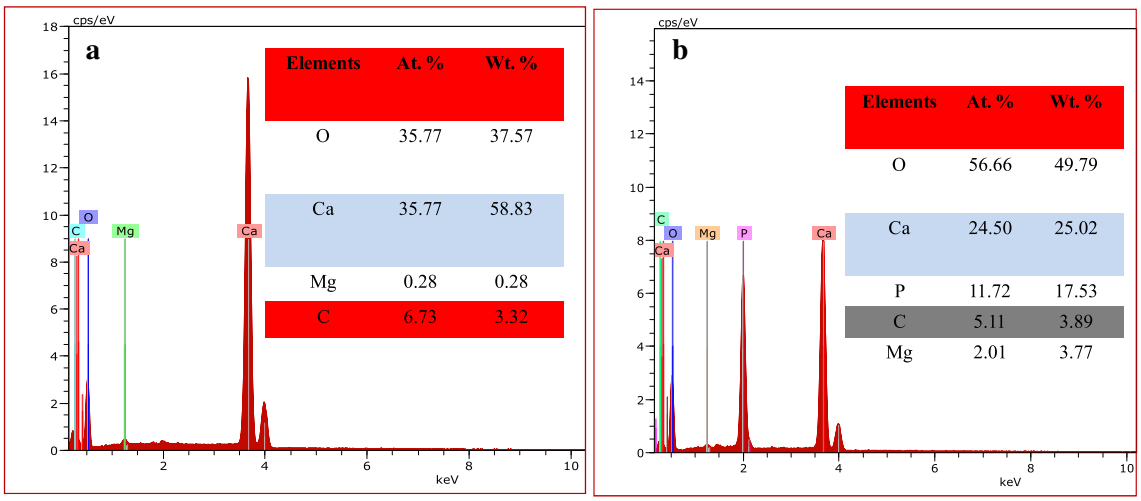


**Fig. 7** EDX of **a** snail shell and **b** carbonated apatite derived from snail shell

Particle size analyses of snail shell powders, as well as the CAP synthesized were carried out and the pattern of particle size distribution is as shown in Fig. 8. Average particle size was found to be 0.7 and 0.6 µm for calcined snail shells and apatite powder synthesized respectively. The synthesized apatite seems to have smaller particle size when compared with its precursor material. A small amount of particles in the range of 0·2–0·5 µm were also present in the powder. From the TGA analysis in Fig. 8c, three weight loss regions were observed. First, the weight

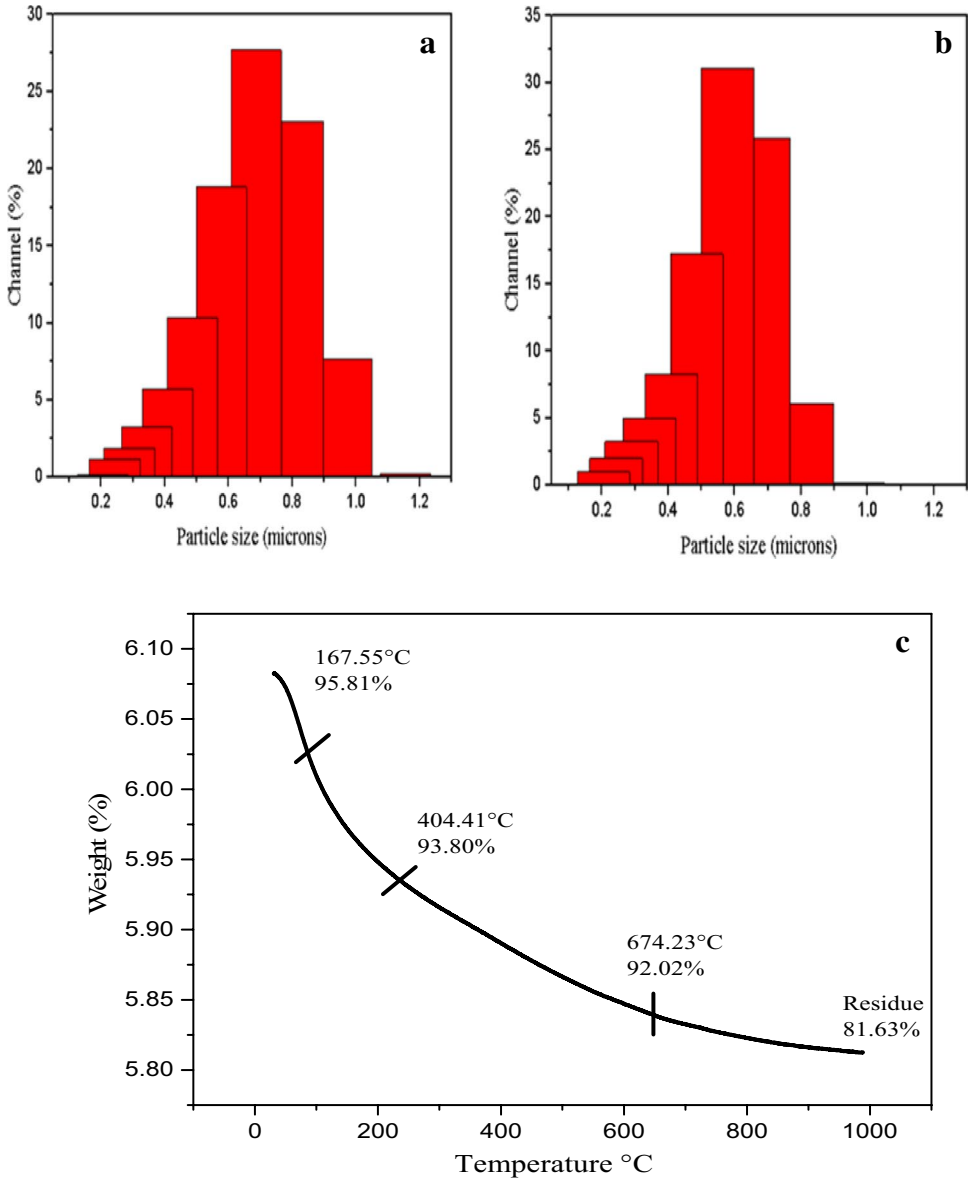


**Fig. 8** particle size distribution of **a** snail shell powder, **b** carbonated apatite powder and **c** TGA analysis of snail shell powder

lost that occurred at around 156.57 °C which is owing to the elimination of moisture and physically adsorbed water molecules from the snail shell. The second loss observed at 540 °C is due to the decomposition of $MgCO_3$ combined with the combustion of hydrocarbons. According to literature report by Mahon et al. [33], $MgCO_3$ decomposition occurs within the temperature range of 433–441 °C. The presence of Mg was observed in the EDX measurement (Fig. 7b). The third weight loss at 700 °C indicates the decomposition of $CaCO_3$ to form calcium oxide and carbon (IV) oxide. However, no significant weight loss was recognized from 800 °C and above which indicate thermal stability of the snail shell. A total residue percentage of 81.63% was achieved.

### 3.2 Scaffold CAP-AMB composite

The structural morphologies of the scaffold surface of CAP-AMB-composites at various concentration of AMB are as depicted in Fig. 9. The images revealed porous structures with increase interconnected pore as the concentration of AMB increases. The carbon content of the scaffold was examines using EDX as listed in Fig. 9d which showed that the scaffold contains carbon contents of 5.03 wt.% and 3.21 at%. The densities of green and sintered CAP-AMB-composite with different concentrations of AMB are as presented in Fig. 10a. It was observed that the density of the composite reduces with a raise in the concentrations of the pore forming agent which is as a result of the replacement of CAP by the pore forming agent. The impact of ammonium bicarbonate on the densification and porosity

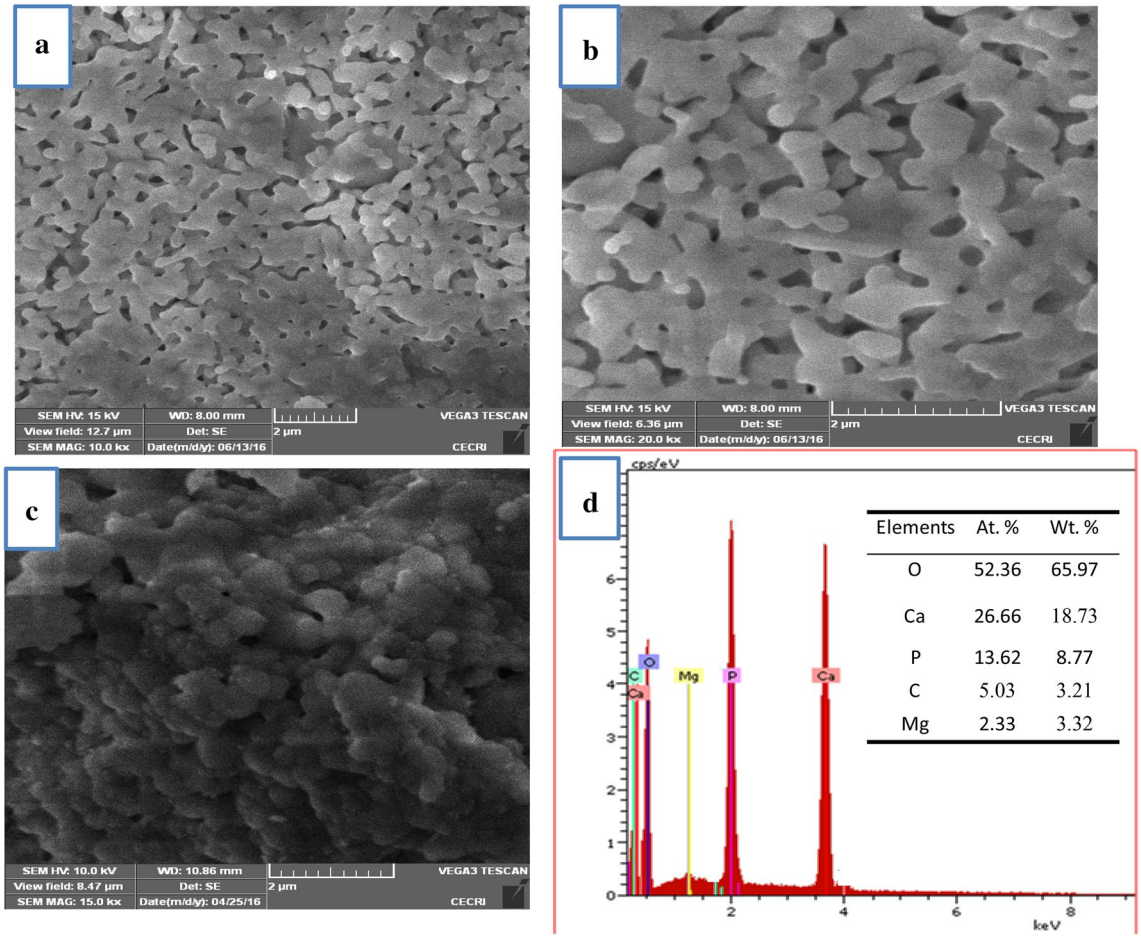


**Fig. 9** SEM images of scaffold at **a** 20%, **b** 30% and **c** 0% (control) AMB, **d** EDX of scaffold prepared

of the snail shell-derived CAP scaffold is represented in Fig. 10b. The density of the nano-composite decline with rise in the concentration of the pore-forming agent, while there was an enormous increase in the porosities of the CAP scaffold. Porosities of 35% and 67% were obtained for AMB concentration of 30% and 50 wt.% respectively. The degrees of porosity could lead to the formation interconnected porous apatite which improves the ingrowth of cells in the porous structure, vascularization, and transport of metabolic products which are crucial for biocompatibility [34]. Figure 10c represents the plots of mercury porosimeter of the snail shell derived scaffold which was found to be in the range of 20 to 100 µm.

### 3.3 Bioactivity study

The bioactivities of the fabricated CAP-AMB porous scaffolds was examined after simulated body fluid soaking for seven days at 37 °C and solution pH of 7.4 by scanning electron microscopy as presented in Fig. 11 which reveals the development of apatite at the porous sites of the scaffold CAP-AMB composite surface. As depicted in Fig. 12a, it was observed that in the course of SBF immersion of CAP-AMB scaffold, the Ca ions concentrations in the SBF media increased with immersion time until it becomes uniform which could be as a result of the precipitation of a calcium phosphate layer. This confirms the diffusion of Ca ions from the CAP-AMB scaffold surface into the SBF media and thereby increasing the Ca ions concentration in the solution. The phosphate ions concentration on the other hand however showed gradual decrease with an increase in the soaking period as indicated in Fig. 12b due to the deposition of phosphate ions on the surface of the apatite [35]. From Fig. 12c, the pH value of the SBF media rose from 7.4 (normal pH of SBF solution) to 8.2 when the soaking time was adjusted from 0 to 7 days. This could be as a result of the swap between the cations present on the surface of the CAP-AMB composite and the hydrogen ions of the SBF media at the CAP-AMB/SBF interface that led to a rise in the value of the SBF solution pH. Sooksaen et al.

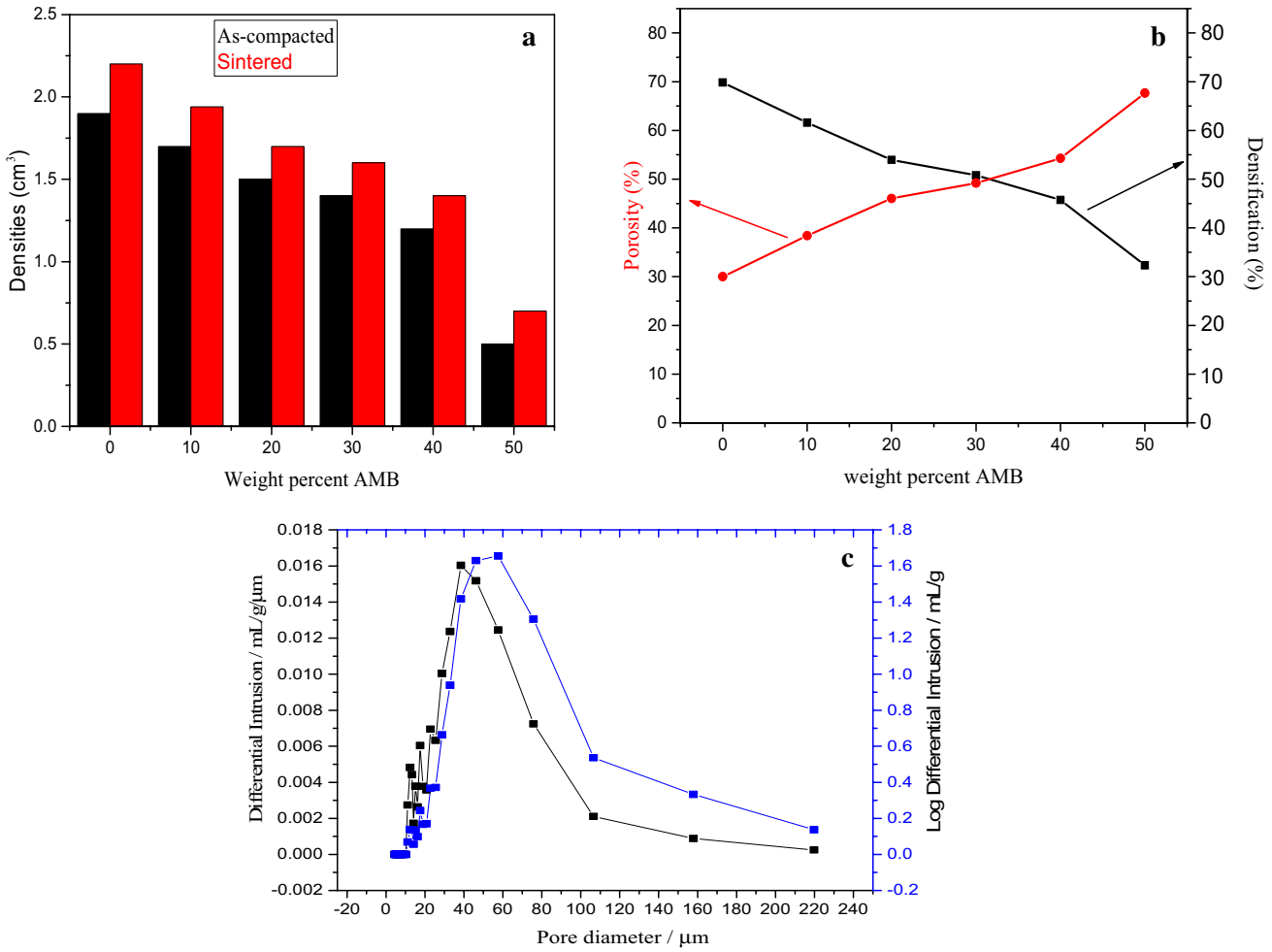


**Fig. 10** Plots of **a** density against weight percent of scaffold CAP-AMB at a compaction pressure of 75 Mpa, **b** porosity and densification against weight percent of ammonium bicarbonate (AMB) of CAP-AMB composite and **c** mercury porosimeter of the porosity of the fabricated scaffold

[36] reported an increase in Ca ions concentration from 83.6 ppm at 0 day to 199.3 ppm after 28 days of soaking and also increase in pH value of SBF solution from 7.40 at 0 day to 8.36 after immersion in SBF for 28 days. After SBF treatment for four days, the EDX elemental analysis of the scaffold surface revealed that the same elements as those before SBF treatment were observed only with an improved Ca values (see Fig. 13). Upon SBF treatment for 7 days, the EDX was able to detect small amounts of elements such as Na and K with an increase in Mg ions concentration plus Ca, P, O and C observed in the CAP-AMB scaffold before SBF treatment as revealed in Fig. 13. Furthermore, there was an improvement in the value of Ca contents thus suggesting the development of Ca-rich amorphous calcium phosphate (ACP) [37]. The spherical particles evidence on the surface of the SBF soaked CAP-AMB scaffold was examined using FT-IR as shown in Fig. 14. From this FT-IR analysis, hydroxyls stretching which ranged from 3465 to 3650 $cm^{-1}$ and at 1650 $cm^{-1}$ were detected. The peaks observed between 3465 to 3650 $cm^{-1}$ splits into two after soaking in SBF solution. Bands corresponding to $PO_4^{3-}$ group were observed between 1055 to 1065 $cm^{-1}$ [6].

## 4 Discussions

This present study demonstrated a novel approach to fabricate CAP and CAP-AMB scaffold composite formed from waste snail shell. The CAP formed was combined with ammonium bicarbonate to improve the biological stability by enhancing its porosity to reach the demand of an application in the bone graft material. It is well known that scaffolds will not only serve as a delivery vehicle for growth factors and living cells but to equally support and regulate bone formation [38]. To facilitate the migration of vascular

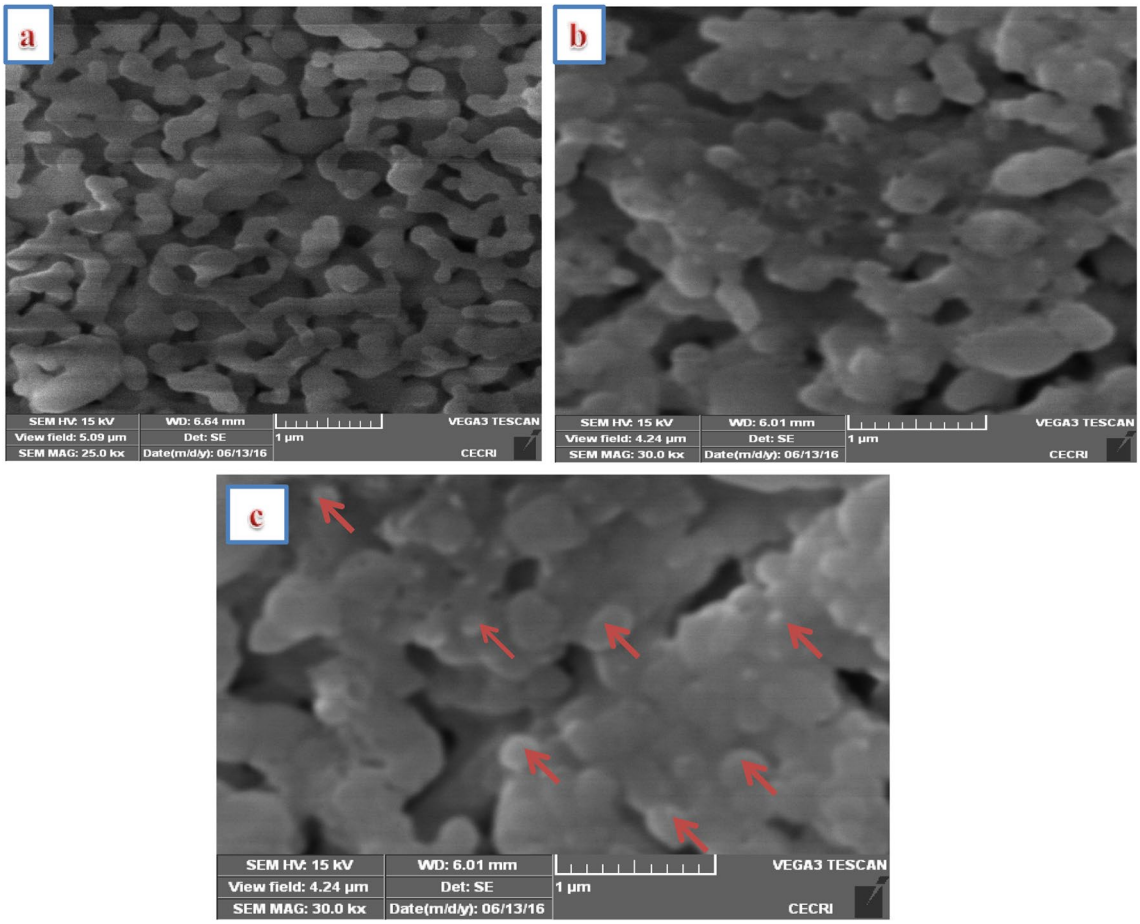


**Fig. 11** SEM images of **a** CAP scaffold, **b**, **c** CAP scaffold in SBF solution after 5 and 7 days of immersion at pH of 7.4 and temperature of 37 °C

tissue and ingrowth of cells, porous structure is desired [39, 40]. From the reports of SEM images of the scaffolds prepared in this study, the CAP-AMB demonstrated porous and interconnected structure which could allow the attachment of cells during biological applications. Porosities of 35% and 67% at AMB concentration of 30% and 50 wt.% respectively with pore size in the range of 60–250 µm were formed. These pore sizes had sufficient space for cells infiltration. According to Sherman and Maretaningtias [40], highly porous and interconnected pore structures were required to ensure that the biological environment is conductive to cell attachment, proliferation, tissue growth and adequate nutrient flow. Thus, to improve bone formation ability, growth factors are needed and these growth factors participate in the regulation of cell proliferation, differentiation, and bone metabolism [39, 40]. Osteoblasts differentiation and matrix mineralization are regulated by the actions of systemic and local signaling factors [39, 40].

The substitution of $CO_3^{2-}$ in the CAP structure can take place at the position of either hydroxyl or that of the phosphate ion position leading to the formation of A and B-type of carbonated CAP [9, 10, 29]. In case of the A-type, the carbonate group showed absorption at around 1550 $cm^{-1}$, 1459 $cm^{-1}$ and 882 $cm^{-1}$ while vibrations at 1464 $cm^{-1}$, 1416 $cm^{-1}$ and 877 $cm^{-1}$ suggests the presence of the B-type carbonate [6, 9, 30]. From this present work, the occurrence of vibration bands at 882 $cm^{-1}$ and 1484 $cm^{-1}$ affirmed the fabricated apatite to be a B-type carbonated apatite in which the phosphate groups of the apatite is substituted with carbonate ions. It is remarkable to note the occurrence of apatite formation around the pores regions of the SBF soaked scaffold. Spherical deposition indicating apatite nucleations were seen in the tested samples. It was reported that apatite deposition begins on the porous site containing well-interconnected pores [6]. A close glance at the images of the soaked CAP-AMB showed that the pores on the surface are enclosed by deposits of apatite. Similar report has been documented in literature [6]. Carbonate bands were detected at 884 and 1488 $cm^{-1}$ with an increase of the latter peak. The SBF treatment of the scaffolds brought about some changes in the FT-IR spectra which is obvious from the shift in peaks positions

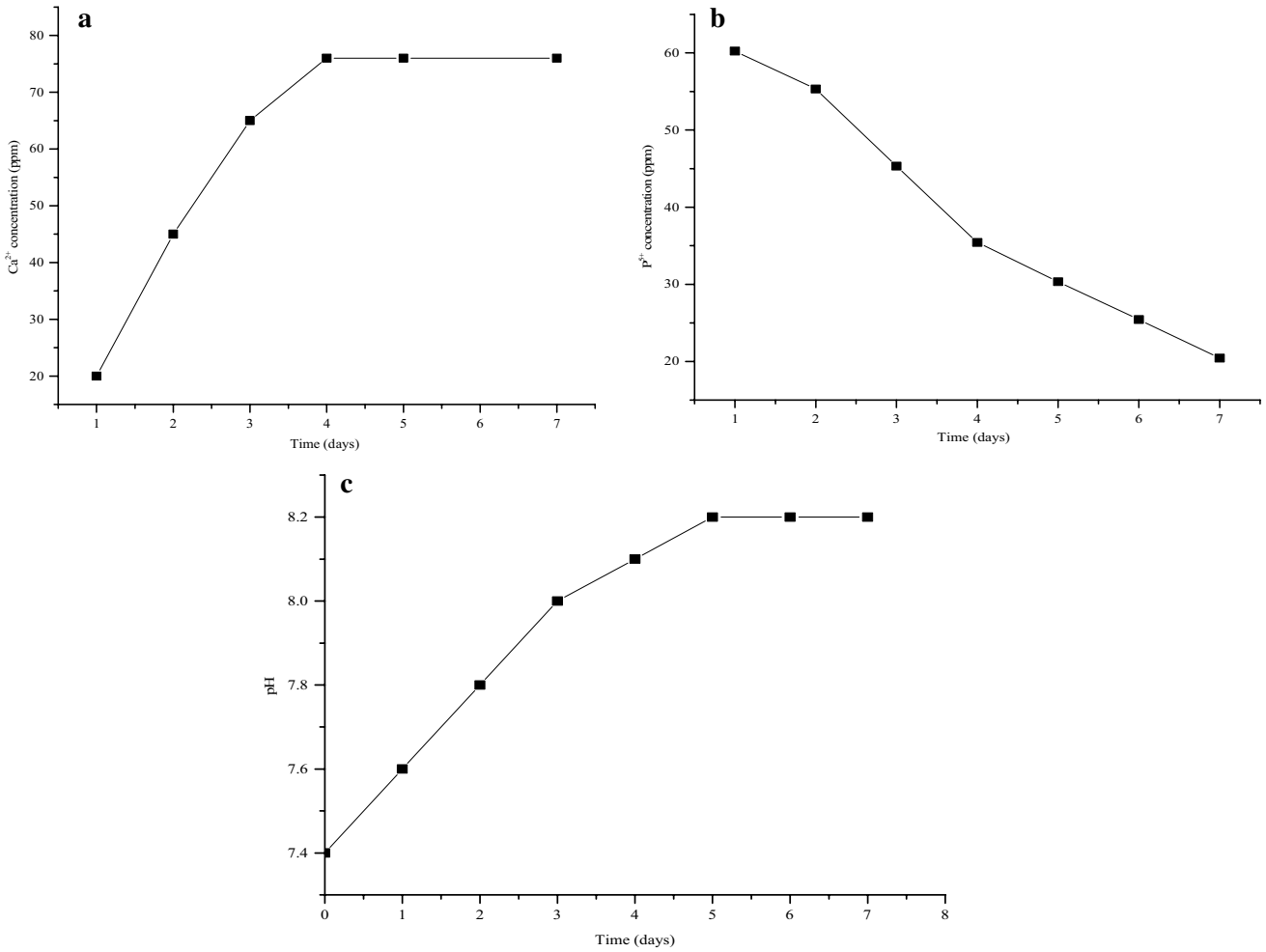


**Fig. 12** Concentrations of **a** $Ca^{2+}$, **b** $P^{5+}$ and **c** pH of SBF solution after 7 days of immersion in SBF 7.4 and temperature of 37 °C

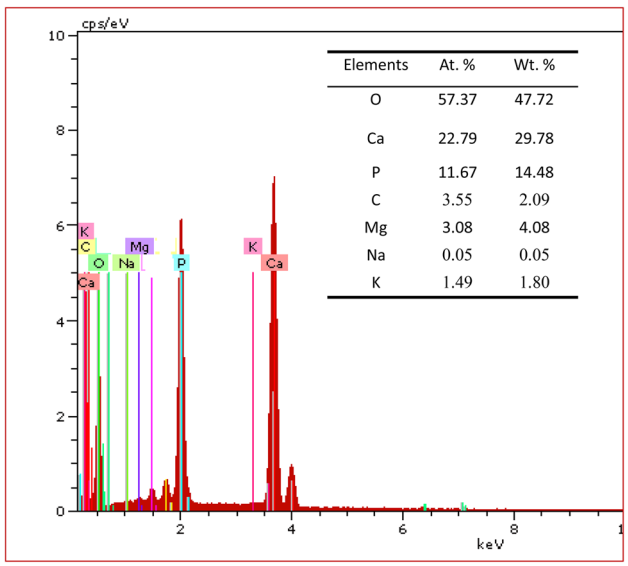


| Elements | At. % | Wt. % |
|---|---|---|
| O | 57.37 | 47.72 |
| Ca | 22.79 | 29.78 |
| P | 11.67 | 14.48 |
| C | 3.55 | 2.09 |
| Mg | 3.08 | 4.08 |
| Na | 0.05 | 0.05 |
| K | 1.49 | 1.80 |

**Fig. 13** EDX of SBF treated CAP-AMB scafold after 7 days of SBF treatment at pH of 7.4 and temperature of 37 °C

of phosphate, carbonate, and hydroxyl groups [6]. This suggests that these functional groups were involved in bond formation with the SBF media of the CAP-AMB scaffold during the one week SBF treatment. The large number of negative ions (i.e. $OH^-$ and $PO_4^{3-}$) on the surface of the apatite determines its' process of formation. During the soaking stage, the cations such as $Ca^{2+}$ ions present in the SBF solution get trapped by the anions such as $OH^-$ and $PO_4^{3-}$ on the surface of the CAP. Thus, the surface acquires positive charge which then draws the negatively charged $OH^-$ and $PO_4^{3-}$ ions from the SBF solution. This results in the formation of the layers of apatite [35]. Pradnya et al. [41] noted that an SBF incubated material formed layers of apatite on the scaffold surface which passes through several chemical reactions such as nucleation, growth of calcium phosphate, spontaneous precipitation. Since surface chemistry plays vital role in the bone bonding property, the various functional groups as observed in the FT-IR analysis (such as $CO_3^{2-}$, $PO_4^{3-}$ and the OH groups) are thus

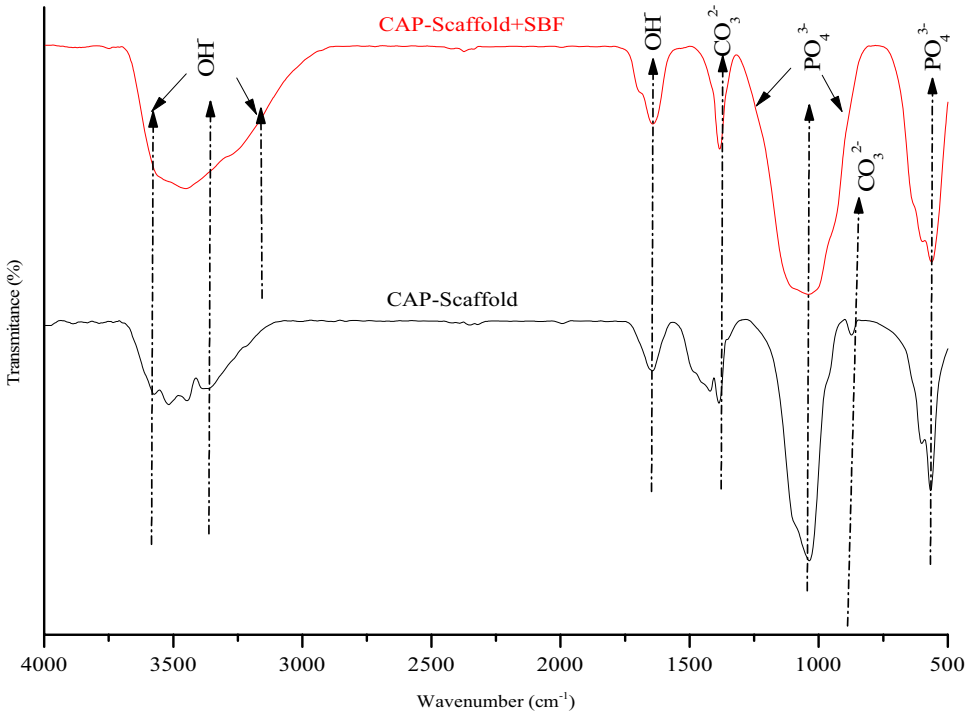


**Fig. 14** FT-IR spectra of CAP-AMB scaffold before and after immersion in SBF solution for 7 days at pH of 7.4 and temperature of 37 °C

accountable for the electrostatic interaction between the surface of the apatite and the SBF solution.

## 5 Conclusions

In this study, waste snail shell was utilized for the synthesis of carbonated apatite powder via thermal and chemical precipitation methods. XRD analysis showed that the fabricated apatite is monophasis apatite, while well resolved characteristic peaks of phosphate and hydroxyl groups were observed from the FT-IR analysis. The appearance of vibration bands at 882 $cm^{-1}$ and 1484 $cm^{-1}$ indicates the formation of a B-type carbonated apatite. Based on Fe-SEM and TEM micrographs, it was found that the morphology of the as-prepared CAP contained different particle sizes and shapes (rod-like, capsule-like and round shapes) crystals. The reaction of the fabricated carbonated apatite powder with ammonium bicarbonate produced porous and interconnected scaffolds with porosity of 35% and 67% respectively. Bioactivity study revealed that the scaffold showed excellent bioactivity ability with the formation of bone-like apatite after seven days of SBF soaking. The concentration of $Ca^{2+}$ ions of the SBF media increases while that of its phosphate ions counterpart decreases. Thus, waste biomaterial of snail shell was utilized for the synthesis of carbonated apatite powder which demonstrated excellent bioactivity in simulated body fluid.

**Acknowledgements** Authors sincerely appreciate the technical staff of CSIR-CECRI, Central Instrumentation Facility staff: Ms Nalini (SEM in charge), Mr R. Ravishankar and Mr A. Rathish Kumar (TEM in charge), Karaikudi, Tamil Nadu, India for their help and support during the characterization. Author Ofudje E.A. acknowledges the financial assistance obtained from the Department of Science and Technology, Government of India through the RTF-DCS (DST) fellowship.

**Funding** This research study was financially supported by the Department of Science and Technology, Government of India through the RTF-DCS (DST) fellowship.

## Declarations

**Conflict of interest** The authors do disclosed that no competing interests exit.

## References


1. Muhammad A, Rashid A, Imran S, Wan AWI, Rafaqat H (2014) Extracting hydroxyapatite and its precursors from natural resources. J Mater Sci 49:1461–1475
2. Rey C, Renugopalakrishnan V, Shimizu M, Collins B, Glimcher MJ (1991) A resolution-enhanced fourier transform infrared spectroscopic study of the environment of the $CO_3^{2-}$ ion in the mineral phase of enamel during its formation and maturation. Calcif Tissue Int 49(4):259–268
3. Doi Y, Moriwaki Y, Okazaki M, Tokahashi J, Joshin K (1982) Carbonate apatite from aqueous and non-aqueous media studied by ESR, IR and X-ray diffraction: effect of $NH_4^+$ ions on crystallographic parameters. J Dent Res 61:429–434
4. Landia E, Celottia G, Logroscinob G, Tampieria A (2003) Carbonated hydroxyapatite as bone substitute. J Eur Ceram Soc 23:2931–2937
5. Solonenko A, Golovanova OA (2014) Silicate_substituted carbonated hydroxyapatite powders prepared by precipitation from aqueous solutions. Russ J Inorg Chem 59(11):1228–1236
6. Ofudje EA, Rajendran A, Adeogun AI, Idowu MA, Kareem SO, Pattanayak DK (2017) Synthesis of organic derived hydroxyapatite scaffold from pig bone waste for tissue engineering applications. Adv Powder Technol. https://doi.org/10.1016/j.apt.2017.09.008
7. Le Geros RZ (1991) Calcium phosphates in oral biology and medicine. In: Myers Karger H (ed) Monographs in oral science. AG Publishers, Basel, pp 82–107
8. Venkatesan J, Qian ZJ, Ryu M, Thomas NV, Kim SK (2011) A comparative study of thermal calcination and an alkaline hydrolysis method in the isolation of hydroxyapatite from *Thunnus obesus* bone. Biomad Mater 6(035003):12
9. Suresh KG, Sathish L, Govindan R, Girija EK (2015) Utilization of snail shells to synthesis hydroxyapatite nanorods for orthopedic applications. RSC Adv 5:39544
10. Adeogun AI, Ofudje EA, Idowu MA, Kareem SO (2017) Facile development of nano size calcium hydroxyapatite based ceramic from eggshells synthesis and characterization. Waste Biomass Valor. https://doi.org/10.1007/s12649-017-9891-3
11. Mustaffa R, Mohd Yusof MR, Abdullah Y (2015) A novelty of synthetic hydroxyapatite from cockle shell and characterization. Adv Mater Res 1087:429–433
12. Santhosh S, Prabu SB (2013) Thermal stability of nano hydroxyapatite synthesized from sea shells through wet chemical synthesis. Mater Lett 97:121–124
13. Walsh PJ, Buchanan FJ, Dring M, Maggs C, Bell S, Walker GM (2008) Low-pressure synthesis and characterisation of hydroxyapatite derived from mineralise red algae. Chem Eng J 137:173–179
14. Rosita W, Yusril Y (2019) Carbonated hydroxyapatite derived from *Cerastoderma edule, Paphia undulata,* and *Meretrix meretrix* shells. IOP Conf Series 546(2019):042049. https://doi.org/10.1088/1757-899X/546/4/042049
15. Kumar GS, Sathish L, Govindan R, Girija EK (2015) Utilization of snail shells to synthesise hydroxyapatite nanorods for orthopedic application. RSC Adv 5:39544–39548. https://doi.org/10.1039/C5RA04402B
16. Huan Z, Mengmeng Y, Mingjie Z, Saisai H, Shiqin K, Lei Y, Linhong D (2016) Preparation of Chinese mystery snail shells derived hydroxyapatite with different morphology using condensed phosphate sources. Ceram Int. https://doi.org/10.1016/j.ceramint.2016.07.101
17. Ogogo AU, Ijeomah HM, Ekwere IF (2010) A survey of snail farms in cross river state, Nigeria. Glob App Extension Prac 6(1):48–57
18. Agbaji C (2018) Snail farming business venture. Leadership newspaper, Published July 6, 2018. https://leadership.ng/2018/07/06/snail-farming-business-venture/. Accessed 28 Feb 2020
19. Tobins FH, Abubakre OK, Muriana RA, Abdulrahman SA (2018) Snail shell as an inspiring engineering material in science and technology development: a review. Int J Contemp Res Rev 9(3):20408–20416
20. Kolawole MY, Aweda JO, Abdulkareem S (2017) Archachatina marginata bio-shells as reinforcement materials in metal matrix composites. Int J Automot Mech Eng 14(1):4068–4079
21. Edokpayi JN, Odiyo JO, Popoola EO, Alayande OS, Msagati TAM (2015) Synthesis and characterization of biopolymeric chitosan derived from land snail shells and its potential for Pb2+ removal from aqueous solution. Materials 8:8630–8640. https://doi.org/10.3390/ma8125482
22. Rao VK, Kumar JSK, Reddy MVB, Murthy CVN (2016) Determination of calcium content in shells of gastropod snails Ramayapatnam beach of Andhra Pradesh. J Chem Pharm Res 8(8):577–580
23. Asafa TB, Durowoju MO, Oyewole AA, Solomon SO, Adegoke RM, Aremu OJ (2015) Potentials of snail shell as reinforcement for discarded aluminum based materials. Int J Adv Sci Technol 84:1–8
24. Teerawat L, Ratchawoot S, Patamaporn C, Sukangkana T, Apichat B, Prinya C (2021) Calcium phosphate powders synthesized from CaCO3 and CaO of natural origin using mechanical activation in different media combined with solid-state interaction. Mater Sci Eng C 118:111333. https://doi.org/10.1016/j.msec.2020.111333
25. Ofudje EA, Adeogun AI, Idowu MA, Kareem SO (2019) Synthesis and characterization of Zn-doped hydroxyapatite: scaffold application, antibacterial and bioactivity studies. Heliyon 4:e01716. https://doi.org/10.1016/j.heliyon.2019.e01716
26. Kokubo T, Takadama H (2009) How useful is SBF in predicting in vivo bone bioactivity? Biomaterials 27:2907–2915
27. Briak-BenAbdeslam HE, Mochales C, Ginebra MP, Nurit J, Planell JA, Boudeville P (2003) Dry mechanochemical synthesis of hydroxyapatites from dicalcium phosphate dihydrate and calcium oxide: a kinetic study. J Biomed Mater Res A 67:927–937
28. Laonapakul T, Sutthi R, Chaikool P, Talangkun S, Boonma A, Chindaprasirt P (2021) Calcium phosphate powders synthesized from CaCO3 and CaO of natural origin using mechanical activation in different media combined with solidstate interaction. Mater Sci Eng C 118:111333
29. Wahyudi ST, Dewi SU, Anggraeni A, Dahlan K, Akhmalok M, Zulfikar A, Hertadi R (2014) Simple and easy method to synthesize chicken eggshell based hydroxyapatite. Adv Mater Res 896:276–279
30. Zhou W, Wang M, Cheung W, Guo B, Jia D (2008) Synthesis of carbonated hydroxyapatite nanospheres through nanoemulsion. J Mater Sci 10(1):103–110
31. Mohammad A, Rashid A, Imram S, Wan AWI, Rafayat H (2014) Extracting hydroxyapatite and its precursors from natural resources. J Mater Sci 49:1461–1475
32. Safronova TV, Putlyaev VI, Avramenko OA, Shekhirev MA, Veresov AG (2011) Cadeficient hydroxyapatite powder for producing tricalcium phosphate based ceramics. Glas Ceram 68:28–32
33. Mahon D, Claudio G, Eames P (2021) An experimental study of the decomposition and carbonation of magnesium carbonate for medium temperature thermochemical energy storage. Energies 14:1316. https://doi.org/10.3390/en14051316
34. Nouri A, Hodgson PD, and Wen C (2010) Biomimetic porous titanium scaffolds for orthopedic and dental applications, in Biomimetics learning from nature. In-Tech, Rijek, Croatia, pp 415–450. Available from Deakin http://hdl.handle.net/10536/DRO/DU:30034370. Accessed 15 Oct 2019

35. Mohamed KR, Beherei HH, El-Rashidy ZM (2014) In vitro study of nano-hydroxyapatite/chitosan–gelatin composites for bio-applications. J Adv Res 5:201–208
36. Sooksaen P, Pengsuwan N, Karawatthanaworraku S, Pianpraditkul S (2015) Formation of porous apatite layer during in vitro study of hydroxyapatite-AW based glass composites. Adv Condens Matter Phys. https://doi.org/10.1155/2015/158582
37. Kim H-M, Himeno T, Kawashita M, Kokubo T, Nakamura T (2004) The mechanism of biomineralization of bone-like apatite on synthetic hydroxyapatite: an in vitro assessment. J R Soc Interface 2004(1):17–22. https://doi.org/10.1098/rsif.2004.0003
38. Mathew PN, Binulala SV, Selvamurugana N, Tamurac H, Jayakumara R (2010) Novel biodegradable chitosan/gelatin/nano-bioactive glass ceramic composite scaffolds for alveolar bone tissue engineering. Chem Eng J 158:353–361
39. Wang L, Huang Y, Pan K, Jiang X, Liu C (2010) Osteogenic responses to different concentrations/ratios of BMP-2 and bFGF in bone formation. Ann Biomed Eng 38:77–87
40. Sherman S, Maretaningtias DA (2015) In vitro and in vivo evaluation of carbonate apatite-collagen scaffolds with some cytokines for bone tissue engineering. J Indian Prosthodont Soc 15(4):349–355
41. Pradnya NC, Manjushri MB, Ravindra UM, Megha PM, Rajendra SK (2010) Study of nanobiomaterial hydroxyapatite in simulated body fluid: formation and growth of apatite. Mater Sci Eng B 168:224–230